Journal of Biomedical Optics 12(2), 1 (March/April 2007)

Early spectral changes of cellular malignant transformation using Fourier transform infrared microspectroscopy

Evgeny Bogomolny
Ben Gurion University
Department of Physics
Beer-Sheva 84105, Israel

Mahmoud Huleihel
Yelena Suproun
Ben-Gurion University of the Negev
Medical School
Department of Virology and Developmental Genetics
Beer-Sheva 84105, Israel

Ranjit K. Sahu*
Shaul Mordechai
Ben Gurion University
Department of Physics
Beer-Sheva 84105, Israel
E-mail: shaulm@bgu.ac.il

Abstract. Fourier transform infrared microspectroscopy (FTIR-MSP) is potentially a powerful analytical method for identifying the spectral properties of biological activity in cells. The goal of the present research is the implementation of FTIR-MSP to study early spectral changes accompanying malignant transformation of cells. As a model system, cells in culture are infected by the murine sarcoma virus (MuSV), which induces malignant transformation. The spectral measurements are taken at various postinfection time intervals. To follow up systematically the progress of the spectral changes at early stages of cell transformation, it is essential first to determine and validate consistent and significant spectral parameters (biomarkers), which can evidently discriminate between normal and cancerous cells. Early stages of cell transformation are classified by an array of spectral biomarkers utilizing cluster analysis and discriminant classification function techniques. The classifications indicate that the first spectral changes are detectable much earlier than the first morphological signs of cell transformation. Our results point out that the first spectral signs of malignant transformation are observed on the first and third day of postinfection (PI) (for NIH/3T3 and MEF cell cultures, respectively), while the first visible morphological alterations are observed only on the third and seventh day, respectively. These results strongly support the potential of developing FTIR microspectroscopy as a simple, reagent-free method for early detection of malignancy. [DOI: 10.1117/1.2717186]

Keywords: Fourier transform infrared microspectroscopy; malignant transformation; retroviruses; cluster analysis; discriminant classification function.

Paper 06194R received Jul. 25, 2006; revised manuscript received Dec. 21, 2006; accepted for publication Jan. 12, 2007.

1 Introduction

Fourier transform infrared (FTIR) microspectroscopy (MSP) has emerged as a powerful tool for chemical analysis because of its ability to provide detailed information on the spatial distribution of chemical composition at the molecular level.[1] In applications requiring qualitative and quantitative analysis, the potential of IR spectroscopy to identify chemical components via fingerprinting analysis of their vibrational spectrum is unsurpassed. When this capability is coupled to an IR microscope, microspectroscopy of μm size samples and high contrast microscopy of 2-D samples based on chemical mapping become possible. Its applications cover a range of disciplines including material science, forensics, biochemistry, biomedical science, and geochemistry, comprising both basic and applied research goals.[2–6]

Apart from the conventional methods of cancer diagnosis, there is a need to develop new approaches that are safe, noninvasive, and effectively detect malignancy at earliest stages. Early detection of cancer is a guarantee in most cases of an effective treatment and in some cases for a complete cure. FTIR-MSP has shown encouraging trends in the field of cancer diagnosis in the last decade.[7] The differences in the absorbance spectra in the mid-IR region between normal and abnormal tissues have been shown to be a possible criterion for detection and characterization of various types of cancers such as: colon,[8–10] breast,[11] leukemia,[12,13] cervical,[14–20] colorectal,[21] skin,[22,23] brain,[24] prostate,[25,26] and also neck and head tumors.[27] Cell cultures are advantageous and more convenient for basic research,[28–33] compared to "real" tissues due to their homogeneity and the ability to control important culture parameters such as growth and malignant transformation rate. Moreover, malignant metamorphose can be monitored by light microscope, in parallel to the spectral measurements. Thus, cell cultures provide an ideal model for detecting early cellular changes during cell transformation.

*Current affiliation: AECOM, Department of Physiology and Biophysics, 1300 Morris Park Avenue, New York, New York 10461.
Address all correspondence to Shaul Mordechai, Physics, Ben-Gurion Univ. of the Negev, Sderot Ben Gurion, Beer Sheva, Negev 84105 Isreal; Tel: 972 8 646 1749; Fax: 972 8 647 2903; E-mail: shaulm@bgumail.bgu.ac.il

1083-3668/2007/12(2)/1/0/$25.00 © 2007 SPIE

In the present work, we used two different cell cultures: murine fibroblast cell line (NIH/3T3) and mouse embryonic fibroblast (MEF, primary cells) as a model system to study early spectral changes induced by cancerous transformation. For this purpose, we first validated consistent spectral biomarkers that were found in previous studies as good biomarkers for detection of malignancy[34–37] using completely transformed fibroblast cell lines. These biomarkers were then utilized for the follow up of malignant cell transformation progression as a function of postinfection time.

2 Materials and Methods

2.1 *Cells and Viruses*

Murine fibroblast cell lines (NIH/3T3, long-term *in vitro*) and mouse embryonic fibroblast cells (MEF, primary cells) were grown at 37°C in RPMI medium supplemented with 10% newborn calf serum (NBCS) and the antibiotics penicillin, streptomycin, and neomycin.

Clone 124 of TB cells chronically releasing the Moloney murine sarcoma virus (MuSV-124) was used to prepare a virus stock that contained an approximately 30-fold excess of MuSV particles over Moloney murine leukemia virus (MuLV) particles.[38] MuLV and MuSV used in this research were grown on NIH/3T3 cells. The virus concentration was determined by counting the number of foci (ffu-focus-forming units).

2.2 *Cell Infection and Determination of Malignant Transformation*

Monolayers of NIH/3T3 and MEF cells were grown in 9-cm^2 tissue culture plates and treated with 0.8 μg/ml of polybrene (a cationic polymer required for neutralizing the negative charge of the cell membrane) for 24 h before infection with the virus. Free polybrene was then removed, and both types of cells were incubated at 37°C for 2 h with the infecting virus (MuSV-124) at various concentrations in RPMI medium containing 2% of NBCS. The unabsorbed virus particles were removed, fresh medium containing 2% NBCS was added, and the monolayers were incubated at 37°C. After various time intervals, the cell cultures were carefully examined for the appearance of malignant transformed cells by the following methods in parallel:

1. morphological observations
2. growth on soft agar[37]
3. FTIR-MSP measurements.

2.3 *Sample Preparation for Fourier Transform Infrared Microscopy Measurements*

Since ordinary glass slides exhibit strong absorption in the wavelength range of interest, zinc sellenide crystals, which are highly transparent to IR radiation, were used. Cell cultures were washed with a physiological saline solution and picked up from the tissue culture plates after treatment with trypsin (0.25%) for 1 min. The cells were pelleted by centrifugation at 1000 rpm for 5 min. Each pellet was washed twice with saline and resuspended in 100 μl of saline. The number of cells was counted with a hematocytometer, and all tested samples were pelleted again and resuspended in an appropriate volume of saline to give a concentration of 1000 cells/μl. A drop of 1 μl of each sample was placed on a certain area on the zinc sellenide crystal, air dried for 1 h, and measured by FTIR microscopy. The radius of such 1-μl drop was about 1 mm, producing a monolayer of cells with about 10 μm. Figure 1 displays characteristic sites for measurements as observed by a light microscope for normal [Fig. 1(a)] and completely transformed [Fig. 1(b)] murine fibroblast cell line (NIH/3T3).

2.4 *Fourier Transform Infrared Microspectroscopy and Data Acquisition*

Measurements on cell cultures were performed using the FTIR microscope IR scope 2 with a liquid-nitrogen-cooled mercury-cadmium-telluride (MCT) detector, coupled to the FTIR spectrometer (Bruker Equinox model 55/S, OPUS software). To achieve high signal-to-noise ratio (SNR), 128 coadded scans were collected in each measurement in the wavenumber region 800 to 4000 cm^{-1}. The measurement site was circular with a diameter of 100 μm and spectral resolution of 4 cm^{-1} was used. To reduce cell amount variation and guarantee proper comparison between different samples, the following procedures were adopted.

1. Each sample was measured at least five times at different spots.
2. ADC rates were empirically chosen between 2000 to 3000 counts/sec (which allows us to measure areas with similar cellular density).
3. The obtained spectra were baseline corrected using the rubberband method with 64 consecutive points and normalized using *min-max normalization* in OPUS software.[39]

2.5 *Statistical Analysis*

The obtained parameters (biomarkers) were classified using the cluster analysis according to Ward's method[40] and the discriminant classification function (DCF) method.[41,42] The differences were considered significant at $P<0.05$.

3 Results

3.1 *Spectral Differences between Normal and Malignant Cell Lines*

The main objective of this research is to identify and study early changes during malignant transformation using FTIR-MSP. As a first step, it was important to find spectral biomarkers that can discriminate between normal and completely malignant cells.

We analyzed FTIR spectra of 50 different samples of both normal (NIH/3T3) and completely transformed murine fibroblast cell lines (NIH/3T3/MuSV). Two regions with significant and consistent differences were identified at 3000 to 2820 cm^{-1} and 1145 to 1000 cm^{-1}. For an effective comparison, these regions were cut from the entire spectra, normalized, and baseline corrected.

The results in the region 3000 to 2820 cm^{-1}, presented in Fig. 2(a), show four prominent absorbance bands: near 2852 cm^{-1} (due to the symmetric stretching of the methylene chains in membrane lipids); at 2923 cm^{-1} (due to the antisymmetric CH_2 stretch); at 2958 cm^{-1} (due to antisymmetric stretching of the methyl groups of both lipids and proteins); and at 2871 cm^{-1} (arising from the symmetric CH_3 stretching

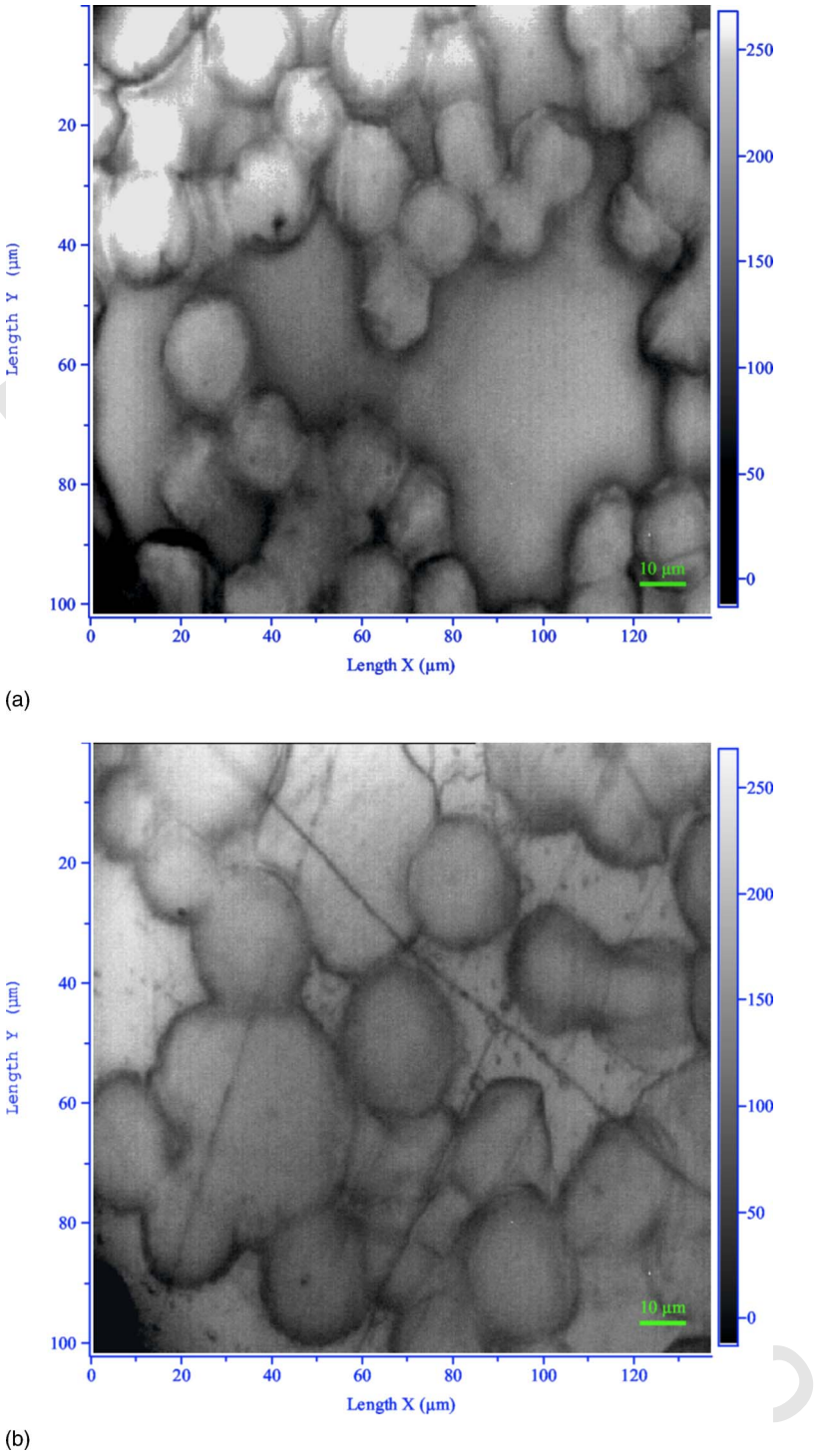

Fig. 1 Photomicrograph of (a) normal NIH/3T3 cell line and (b) completely transformed fibroblast cell line (NIH/MuSV).

mode).[1] The average absorption intensities of normal and transformed fibroblast cell lines are distinctive at 2852-cm^{-1} and 2958-cm^{-1} bands [Fig. 2(a)]. It was found that the best discriminating values were obtained by deriving the intensity ratio of these two vibrational modes (i.e., A_{2958}/A_{2852} or υ_{as} CH_3/υ_s CH_2).

The dimensionless ratio eliminates artifact, which may arise due to the baseline contribution underneath each band. Table 1 summarizes the statistical values of the previous ratio for the normal and malignant cell line. The *t*-value of the two groups is 11.25 (Table 1). Therefore, this ratio may be considered as a satisfactory biomarker to follow the progress of malignant transformation.

In the second region at 1145 to 1000 cm^{-1} [Fig. 2(b)], there are plenty of overlapping vibrational modes associated with absorbance of macromolecules such as proteins, nucleic

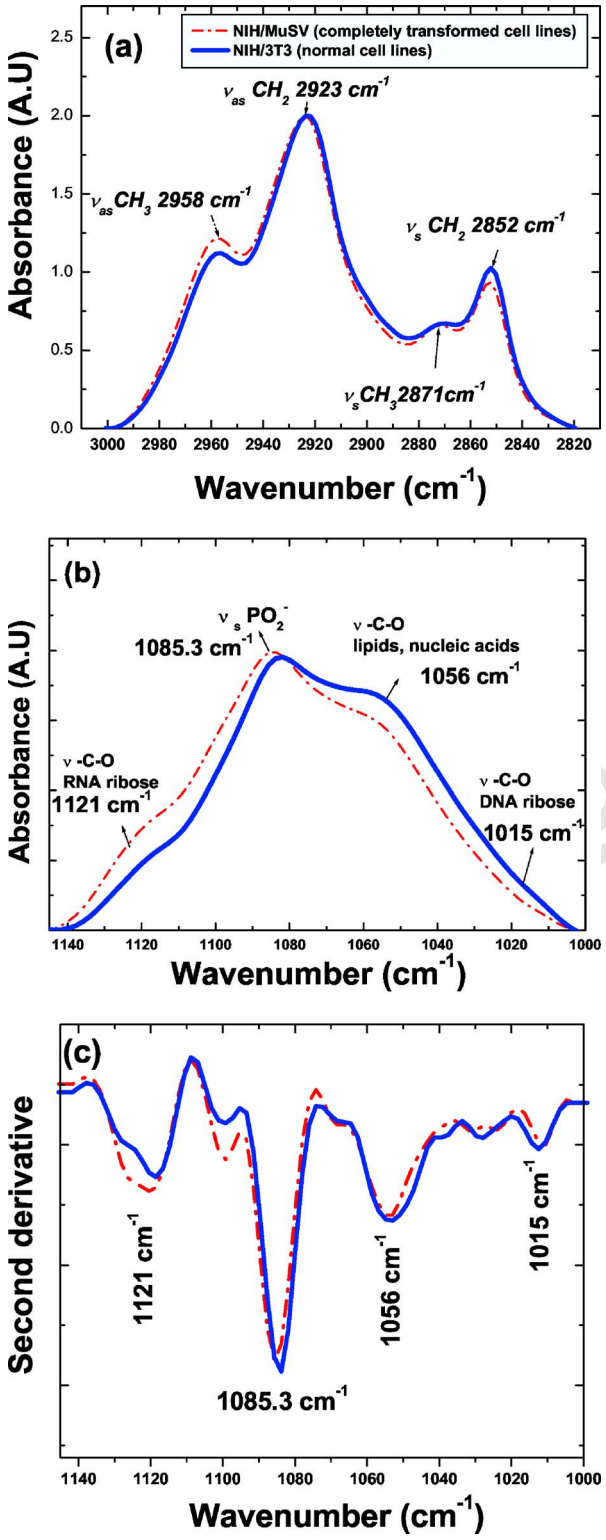

Fig. 2 FTIR spectra in the regions: (a) 2820 to 3000 cm^{-1}, (b) 1000 to 1145 cm^{-1}, and (c) the second derivative at 1000 to 1145 cm^{-1} of the normal murine fibroblast cell line (NIH/3T3) and of the completly transformed murine fibroblast cell line (NIH3T3/MuSV). Spectra are the average of 50 samples and five measurements of each sample after baseline correction and normalization.

166 acids, carbohydrates, and phospholipids. The bands at 1082 and 1056 cm^{-1} correspond to absorbance of the ν_s PO_2^- of 167
phosphodiesters of nucleic acids[1] and the O–H stretching 168
coupled with C–O bending of C–OH groups of carbohydrates, 169
respectively.[39] Other bands at 1121 and 1015 cm^{-1} can be 170
clearly seen in the second derivative spectra [Fig. 2(c)]. Pre- 171
vious works have shown that A_{1121} arises from RNA absor- 172
bance, whereas the 1015 cm^{-1} shoulder is due to DNA.[43–45] 173

From this region it is possible to derive two additional 174
spectral biomarkers with outstanding statistical characteris- 175
tics: A_{1121}/A_{1015} ratio (assigned as RNA/DNA ratio) and the 176
wavenumber shift due to ν_s PO_2^- (relative to 1082 cm^{-1}). 177
Even though the variability of these biomarkers is high due to 178
overlapping absorbance, the average values of normal are still 179
significantly different compared to malignant cells (Table 1). 180

3.2 *Early Stages of Malignant Cell Transformation* 181

Both primary cells (MEF) and murine fibroblast cell lines 182
(NIH/3T3) were infected with MuSV (1 ffu/cell) and exam- 183
ined at various postinfection times for morphological and 184
spectral changes. Figure 3 shows the expanded spectra of both 185
cell cultures in the two wavenumber regions. This figure 186
clearly demonstrates the gradual spectral variations following 187
cell infection. Dramatic changes are observable in the case of 188
MEF transformation, where the band at 1056 cm^{-1} decreases 189
gradually and the band at 1082 cm^{-1} is shifted systematically 190
to higher wavenumbers versus infection time [Fig. 3(d)]. 191
Thus, it is possible to determine the first spectral signs of 192
malignancy according to the alterations in the calculated val- 193
ues of the previously discussed biomarkers. The observed 194
spectral changes in malignant cells compared to control cells 195
are summarized in Table 2. As can be seen in Table 2, the first 196
morphological changes confirmed by microscopical observa- 197
tions and growth on soft agar appear considerably later than 198
the first spectral signs. For example, the first spectral identi- 199
fication is possible on the first day (A_{1121}/A_{1015} biomarker), 200
while morphologically it can be discerned on the third day in 201
the case of NIH/3T3 cell transformations (Table 2). In the 202
case of MEF primary cells, the spectral changes induced by 203
cell transformation were even more significant compared to 204
those induced in the NIH/3T3 transformation [Fig. 3(b)]. Also 205
in MEF primary cells, the first spectral signs appeared signifi- 206
cantly earlier than the morphological changes (on the third 207
day compared to the seventh day). 208

4 Statistical Analysis 209

4.1 *Cluster Analysis* 210

Cluster analysis was used to classify the infected cells at each 211
postinfection day into cancerous or normal groups. For this 212
classification we utilized a vector array of spectral biomark- 213
ers, which were set as follows: 214

$$\begin{pmatrix} A_{2958}/A_{2852} \\ A_{1121}/A_{1015} \\ \text{shift of } \nu_s\ PO_2^- \end{pmatrix}. \quad 215$$

The postinfection days of transformations were characterized 216
using the average values of previously derived spectral biom- 217
arkers. 218

Table 1 Statistical analysis of the biomarkers derived from FTIR spectra of normal and transformed murine fibroblast cell lines.

	A_{2958}/A_{2852}		A_{1121}/A_{1015}		Wavenumber shift due to ν_s PO_2^- (relative to 1082 cm^{-1})	
	Normal	Abnormal	Normal	Abnormal	Normal	Abnormal
Mean	1.09	1.27	1.69	4.26	1.75	3.3
SD	0.05	0.06	0.37	0.61	0.21	0.75
T-value	11.25		16.2		8.87	
P-value	$1 \cdot 10^{-10}$		$1.2 \cdot 10^{-13}$		$1.9 \cdot 10^{-8}$	
Max value	1.18	1.37	2.4	5.53	2.13	4.5
Min value	1.02	1.19	1.21	3.25	1.43	2.12

The results presented in Fig. 4 show that cluster analysis can indeed classify the infected cells into the cancerous group already at the first postinfection day in case of NIH/3T3 cells and at the fifth postinfection day in case of MEF transformation. We note that in both cases, the classifications were significantly earlier than the morphological identification of the malignant cells.

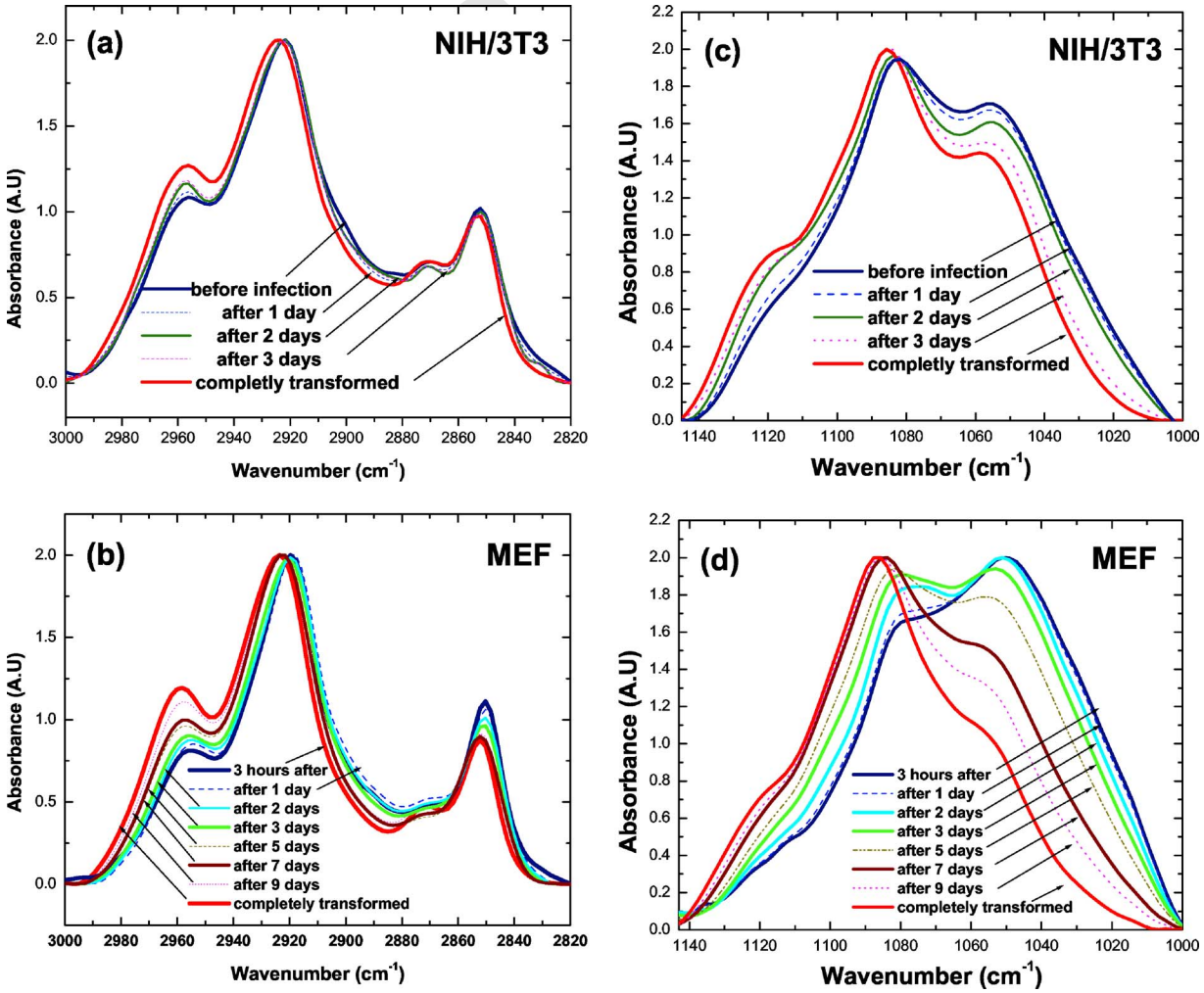

Fig. 3 FTIR spectra of (a) NIH/3T3 and (b) MEF cells at various intervals of postinfection time in the region 2820 to 3000 cm^{-1}. FTIR spectra of (c) NIH/3T3 and (d) MEF cells in various intervals of postinfection time in the region 1000 to 1145 cm^{-1}. Spectra are the average of (a) and (c) 20 transformations of NIH/3T3 cell lines and (b) and (d) 12 transformations of MEF cells.

Table 2 First signs of malignant transformation.

Type of cells in culture	First spectral detection of each biomarker (postinfection day and the percentage changes compared to the control cells)			First morphological signs
	A_{2958}/A_{2852}	A_{1121}/A_{1015}	shift due to ν_s PO_2^-	
NIH/3T3	day 2/8.25±2.7%	day 1 /53.8±11%	day 2/43.2±19%	Day 3
MEF	day 5/32.3±8%	day 3/99.4±23%	day 5/54.3±21%	Day 7

4.2 *Discriminant Classification Function*

Discriminant classification function (DCF) is a statistical tool that enables us to improve discrimination between malignant stages by representing an adequate quantitative follow up of transformations versus time. DCF generates a classification score for each postinfection day, which is a linear combination of previously derived array of biomarkers with weight coefficients,[37,38] as can be seen in the following equation:

$$S = c + w_1 \cdot x_1 + w_2 \cdot x_2 + \ldots + w_m \cdot x_m + \ldots , \quad (234)$$

where w_m is the weight coefficient, x_m is biomarker value, and S denotes the resultant classification score.

The weight coefficients were determined empirically in such a way that they nullify the average classification score of NIH/3T3 array (normal cell score) and yield 100 score (cancerous score) for the average NIH/MuSV array. The same weights were applied also to the MEF transformation. From the DCF analysis, we obtained a classification of the transformations that correspond to a sigmoid fit (Fig. 5). The abnormality can be distinguished as early as the first day in the case of the NIH/3T3 transformation [while first morphological identification is possible on the third day, Fig. 5(a)]. Similarly, Fig. 5(b) shows that the abnormality in the case of MEF transformation is apparent on the third postinfection day (while the first morphological identification is possible on the seventh day). In both cases, the infected cells reach an upper level plateau after full transformation (score of 100 for NIH/3T3 and score of 137 for cancerous MEF, Fig. 5).

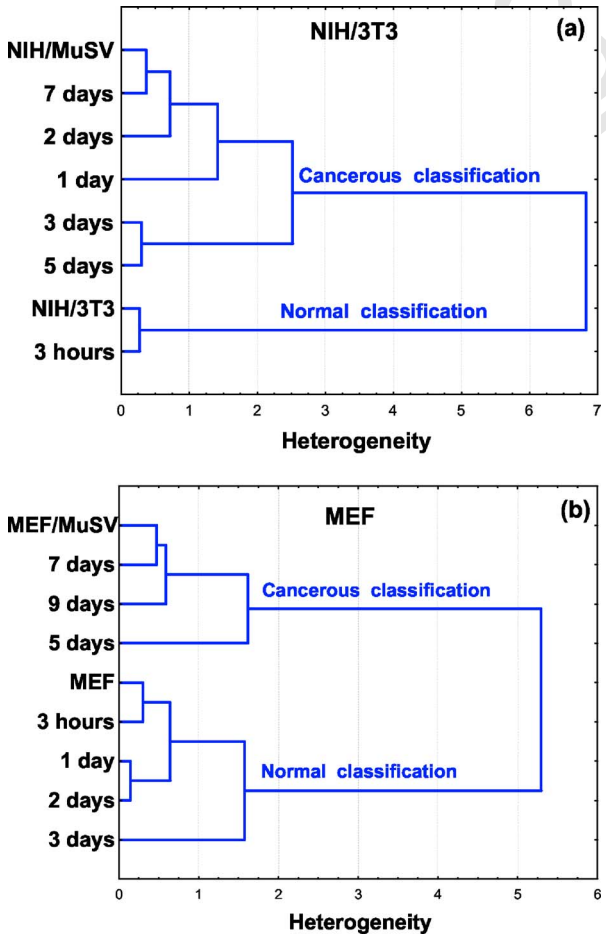

Fig. 4 Cluster analysis of (a) NIH/3T3 and (b) MEF cells at various intervals of postinfection. Cluster analysis is based on the average values of three biomarkers. Each postinfection day of transformation is represented using array of an average value of three biomarkers: (A_{2958}/A_{2852}, A_{1121}/A_{1015}, and the shift of ν_s PO_2^-).

5 Discussion

In the present work, we implemented FTIR-MSP to study the spectral changes of cancerous transformation *in vitro* and focused mainly on early detection of malignancy. For this purpose we utilized an array of spectral biomarkers (A_{2958}/A_{2852}, A_{1121}/A_{1015}, and the wavenumber shift due to ν_s PO_2^-). The obtained results revealed that three FTIR spectral indicators consistently altered during the malignant transformation and can discern malignancy before morphological changes can be observed. Such spectral alterations were considerably higher and significant in the transformations of primary MEF cells compared to NIH/3T3 cell line transformations. Most of the biological characteristics of primary cells are completely different from those of cell lines; they replicate slowly in culture and are very sensitive to the environmental conditions compared to the cell lines. In fact, primary cells are very similar to the normal organism cells in most of their characteristics, while cell lines have some similarity to malignant cells. The gradual changes in these biomarkers during the transformation processes can arise from several cellular activities.

5.1 A_{2958}/A_{2852} (ν_{as} CH_3/ν_s CH_2)

The phospholipids/lipids/triglycerides and proteins absorb in the wavenumber regions from 2800 cm^{-1} to 3000 cm^{-1}.[1,43] Previous studies[46,47] with rat fibroblast cell lines showed that lipids have more predominant absorbance relative to other

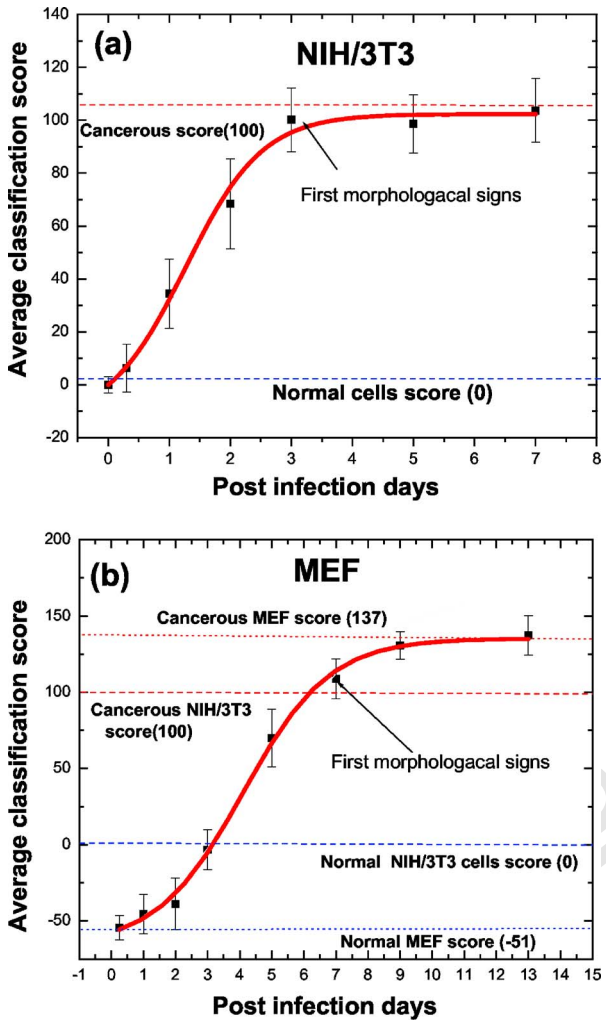

Fig. 5 Discriminant classification function of (a) NIH/3T3 and (b) MEF cells at various intervals of postinfection. Each postinfection day of transformation is represented using an array of average values of three biomarkers: (A_{2958}/A_{2852}, A_{1121}/A_{1015}, and the shift of $\nu_s\ PO_2^-$).

biomolecules, including proteins, at the 2800- to 300-cm^{-1} region. Also, changes in the absorbance due to $\nu_s\ CH_2$ and $\nu_{as}\ CH_3$ vibrational modes of lipids during carcinogenesis were found.[48,49] Our results showed remarkable increment in this ratio in malignant cells compared to normal cell cultures. Similar behavior of this biomarker was observed in leukemia,[50] cervical, colon, and colorectal cancer,[51] as well as in murine fibroblast cell lines and rabbit bone marrow primary cells transformed by MuSV or H-Ras.[50] In addition, the CH_3/CH_2 ratio was found to increase as a function of the progress in malignant lymphoma grade.[52]

Lipids are considered as important components of the cellular membrane, which significantly affect its permeability and metabolites transportation during carcinogenesis,[53] and they also form an influential source of energy that might be essential for malignant metabolism. Moreover, the evidence that transformed cells differ in their average cellular volume compared to the normal cells[54] (Fig. 1) may also contribute to the observed changes seen in the previous ratio.

5.2 A_{1121}/A_{1015} (*RNA/DNA*) *and Wavenumber Shift due to* $\nu_s\ PO_2^-$

The region between 900 to 1200 cm^{-1} has many overlapping bands that correspond to the nucleic acid absorbance.[43–45] Differences in DNA isolated from cancer and normal cells/tissues using FTIR spectroscopy have been the basis of a number of studies for diagnosis of cancer.[55,56] A statistical comparison of the FTIR spectra of DNA obtained from prostate cancer and from normal prostate tissues of healthy younger men revealed a broad array of differences in base structures (e.g., N–H and C–O) as well as in vertical base-stacking interactions and in the phosphodiester-deoxyribose backbone.[55] Also, structural disorders in the pancreatic tumor DNA were detected in the phosphodiester-deoxyribose spectral region.[56]

Our results showed significant increment in the A_{1121}/A_{1015} ratio and $\nu_s\ PO_2^-$ peak shift to higher wavenumbers in malignant compared to normal cell cultures. The utilization of these spectral indicators was widely reported in previous studies.[7–10,12,13,19,20,34–37,57] The same tendency was observed for A_{1121}/A_{1015} ratio in melanoma,[58] leukemia,[12,13] cervical,[19,20] and colon,[7–10,57] cancers as well as murine fibroblast cell lines transformed by MuSV or H-Ras[34–36] and lymphoma.[51,59] In the case of $\nu_s\ PO_2^-$, it was found that the phosphodiester group shifted to higher wavenumbers in various malignant cell cultures such as human primary fibroblast, mouse primary fibroblast, murine fibroblast cell line (NIH/3T3), etc.[37] This shift has been also seen in breast cancer,[60] cancerous stomach tissues,[61] and neoplastic human gastric cells.[62]

It was suggested that the pivotal role of these biomarkers stems from nucleic acid absorbance. The change in the absorbance and conformation of nucleic acids (which can cause a shift in the absorbance of the phosphodiesters group) during carcinogenesis arises from a sharp increment of the proliferation and metabolic activity in the transformed cells and from the high levels of retrovirus DNA and RNA production in the infected or transformed cells. Also, these changes could arise from a variation in the nuclear volume of the transformed cells as previously reported.[63,64] Cell transformation progression in time can be well described by a sigmoid function that was obtained using a discriminant classification function. In a short interval of postinfection time (meaningfully shorter than the cell cycle), there are no detectable spectral differences between infected and control cell cultures. Then the spectral values of the infected cell cultures gradually approach the spectral values of the fully transformed cells (as can be seen in Fig. 5). After obtaining first signs of morphological transformation (as confirmed by microscope and growth on soft agar), all spectral indicators showed identical values to those of the fully transformed cells.

The results presented in this study prove the superiority of FTIR spectroscopy over the conventional technique used for detection of malignant cells in culture. Thus, FTIR-MSP in tandem with proper statistical tools may offer a promising technique for the detection of early stages of malignancy and for monitoring their progression.

Acknowledgments

This research work was supported by the Israel Science Foundation (ISF grant number 788/01) and the Israel Cancer Association (ICA).

References

1. H. Mantsch and D. Chapman, *Infrared Spectroscopy of Biomolecules*, John Wiley, New York (1996).
2. M. Diem, S. Boyston-White, and L. Chiriboga, "Infrared spectroscopy of cells and tissues: Shining light on to a novel subject," *Appl. Spectrosc.* **53**, 148A–161A (1999).
3. D. Naumann, D. Helm, and H. Labischinski, "Microbiological characterizations by FT-IR spectroscopy," *Nature (London)* **351**, 81–82. (1991).
4. H. Gremlich and B. Yang, *Infrared and Raman Spectroscopy of Biological Materials*, Marcel Dekker, New York (2001).
5. P. Lasch, M. Boese, A. Pacifico, and M. Diem, "FT-IR spectroscopic investigations of single cells on the subcellular level," *Vib. Spectrosc.* **28**(1), 147–157 (2002).
6. S. Argov, R. K. Sahu, E. Bernshtain, A. Salman, G. Shohat1, U. Zelig, and S. Mordechai, "Inflammatory bowel diseases as an intermediate stage between normal and cancer: a FTIR-microspectroscopy approach," *Biopolymers* **75**(5), 384–392 (2004).
7. R. K. Sahu and S. Mordechai, "Fourier transform infrared spectroscopy in cancer detection," *Future Oncol.* **1**(5), 635–647 (2005).
8. S. Argov, J. Ramesh, A. Salman, I. Silenikov, J. Goldstein, H. Guterman, and S. Mordechai, "Diagnostic potential of fourier transformed infrared microspectroscopy and advanced computational methods in colon cancer patients," *J. Biomed. Opt.* **7**(2), 248–254 (2002).
9. A. Salman, S. Argov, J. Ramesh, J. Goldstein, I. Silenikov, H. Guterman, and S. Mordechai, "FTIR microscopic characterization of normal and malignant human colonic tissues," *Cell Mol. Biol. (Paris)* **47**(22), 159–166 (2001).
10. R. K. Sahu, S. Argov, E. Bernshtain, A. Salman, S. Walfisch, J. Goldstein, and S. Mordechai, "Detection of abnormal proliferation in histologically 'normal' colonic biopsies using FTIR-microspectroscopy," *Scand. J. Gastroenterol.* **39**(6), 557–566 (2004).
11. T. Gao, J. Feng, and Y. Ci, "Human breast carcinomal tissues display distinctive FTIR spectra: implication for the histological characterization of carcinomas," *Anal. Cell. Pathol.* **18**, 87–93 (1999).
12. R. K. Sahu, U. Zelig, M. Huleihel, N. Brosh, M. Talyshinsky, M. Harosh, S. Mordechai, and J. Kapelushnik, "Continuous monitoring of WBC (biochemistry) in an adult leukemia patient using advanced FTIR-spectroscopy," *Leuk. Res.* **30**(6), 687–693 (2006).
13. J. Ramesh, J. Kapelushnik, J. Mordechai, A. Moser, M. Huleihel, V. Erukhimovitch, C. Levi, and S. Mordechai, "Novel methodology for the follow-up of acute lymphoblastic leukemia using FTIR Microspectroscopy," *J. Biochem. Biophys. Methods* **51**(3), 251–261 (2002).
14. L. Chiriboga, P. Xie, H. Yee, D. Zarou, D. Zakim, and M. Diem, "Infrared spectroscopy of human tissue. IV. Detection of human cervical tissue via infrared microscopy," *Cell Mol. Biol. (Paris)* **44**(1), 219–229 (1998).
15. P. Podshyvalov, R. K. Sahu, S. Mark, K. Kantarovich, H. Guterman, J. Goldstein, J. Ramesh, S. Argov, and S. Mordechai, "Distinction of cervical cancer biopsies by use of infrared microspectroscopy and probabilistic neural networks," *Appl. Opt.* **44**(18), 3725–3734 (2005).
16. W. Steller, J. Einenkel, L. C. Horn, U. D. Braumann, H. Binder, R. Salzer, and C. Kraft, "Delimitation of squamous cell cervical carcinoma using infrared microspectroscopic imaging," *Anal. Bioanal. Chem.* **384**(1), 145–154 (2006).
17. B. R. Wood, L. Chiriboga, D. McNaughton, and M. Diem, "Fourier transform infrared (FTIR) spectral mapping of the cervical transformation zone, and dysplastic squamous epithelium," *Gynecol. Oncol.* **93**(1), 59–68 (2004).
18. J. I. Chang, Y. B. Huang, P. C. Wu, C. C. Chen, S. C. Huang, and Y. H. Tsai, "Characterization of human cervical precancerous tissue through the fourier transform infrared microscopy with mapping method," *Gynecol. Oncol.* **91**(3), 577–583 (2003).
19. S. Mordechai, R. K. Sahu, Z. Hammody, S. Mark, K. Kantarovich, H. Guterman, P. Podshyvalov, J. Goldstein, and S. Argov, "Possible common biomarkers from FTIR microspectroscopy of cervical cancer and melanoma," *J. Microsc.* **215**, 86–91 (2004).
20. S. Mark, R. K. Sahu, K. Kantarovich, P. Podshyvalov, H. Guterman, J. Goldstein, S. Argov, and S. Mordechai, "Fourier transform infrared microspectroscopy as a quantitative diagnostic tool for assignment of premalignancy grading in cervical neoplasia," *J. Biomed. Opt.* **9**(3), 558–567 (2004).
21. P. Lasch, W. Haensch, D. Naumann, and Max Diem, "Imaging of colorectal adenocarcinoma using FT-IR microspectroscopy and cluster analysis," *Biochim. Biophys. Acta* **1668**(2), 176–186 (2004).
22. A. Tfayli, O. Piot, A. Durlach, A. Bernard, and M. Manfait, "Discriminating nevus and melanoma on paraffin-embedded skin biopsies using FTIR microspectroscopy," *Biochim. Biophys. Acta* **1724**(3), 262–269 (2005).
23. N. Eikje, K. Aizawa, and Y. Ozaki, "Vibrational spectroscopy for molecular characterization and diagnosis of benign, premalignant and malignant skin tumours," *Biotechnol. Annu. Rev.* **11**, 191–225 (2005).
24. C. Krafft, L. Shapoval, S. B. Sobottka, K. D. Geiger, G. Schackert, and R. Salzer, "Identification of primary tumors of brain metastases by SIMCA classification of IR spectroscopic images," *Biochim. Biophys. Acta* **1758**(7), 883–891 (2006).
25. E. Gazi, M. Baker, J. Dwyer, N. P. Lockyer, P. Gardner, J. H. Shanks, R. S. Reeve, C. A. Hart, N. W. Clarke, and M. D. Brown, "A correlation of FTIR spectra derived from prostate cancer biopsies with gleason grade and tumour stage," *Eur. Urol.* **50**(4), 750–760 (2006).
26. D. Fernandez, R. Bhargava, S. M. Hewitt, and I. W. Levin, "Infrared spectroscopic imaging for histopathologic recognition," *Nat. Biotechnol.* **23**(4), 469–474 (2005).
27. P. Bruni, C. Conti, E. Giorgini, M. Pisani, C. Rubini, and G. Tosi, "Histological and microscopy FT-IR imaging study on the proliferative activity and angiogenesis in head and neck tumours," *Faraday Discuss.* **126**, 19–26 (2004).
28. M. German, A. Hammiche, N. Ragavan, M. J. Tobin, J. L. Cooper, S. S. Matanhelia, A. C. Hindley, C. M. Nicholson, N. J. Fullwood, H. M. Pollock, and F. L. Martin, "Infrared spectroscopy with multivariate analysis potentially facilitates the segregation of different types of prostate cell," *Biophys. J.* **90**(10), 3783–3795 (2006).
29. Y. Yang, J. Sule-Suso, G. D. Sockalingum, G. Kegelaer, M. Manfait, and A. El Haj, "Study of tumor cell invasion by Fourier transform infrared Microspectroscopy," *Biopolymers* **78**(6), 311–317 (2005).
30. L. Zhang, G. W. Small, A. S. Haka, L. H. Kidder, and E. N. Lewis, "Classification of Fourier transform infrared microscopic imaging data of human breast cells by cluster analysis and artificial neural networks," *Appl. Spectrosc.* **57**(1), 14–22 (2003).
31. J. Sule-Suso, A. Forster, V. Zholobenko, N. Stone, and A. El Haj, "Effects of CaCl2 and MgCl2 on Fourier transform infrared spectra of lung cancer cells," *Appl. Spectrosc.* **58**(1), 61–67 (2004).
32. C. M. Krishna, G. Kegelaer, I. Adt, S. Rubin, V. B. Kartha, M. Manfait, and G. D. Sockalingum, "Combined Fourier transform infrared and Raman spectroscopic approach for identification of multidrug resistance phenotype in cancer cell lines," *Biopolymers* **82**(5), 462–470 (2006).
33. C. M. Krishna, G. D. Sockalingum, R. A. Bhat, L. Venteo, P. Kushtagi, M. Pluot, and M. Manfait, "FTIR and Raman microspectroscopy of normal, benign, and malignant formalin-fixed ovarian tissues," *Anal. Bioanal. Chem.* (in press).
34. M. Huleihel, A. Salman, V. Erukhimovitch, J. Ramesh, Z. Hammody, and S. Mordechai, "Novel spectral method for the study of viral carcinogenesis in vitro," *J. Biochem. Biophys. Methods* **50**(2–3), 111–121 (2002).
35. J. Ramesh, A. Salman, Z. Hammody, B. Cohen, J. Gopas, N. Grossman, and S. Mordechai, "Application of FTIR microscopy for the characterization of malignancy: H-ras transfected murine fibroblasts as an example," *J. Biochem. Biophys. Methods* **50**(1), 33–42 (2001).
36. A. Salman, J. Ramesh, V. Erukhimovitch, M. Talyshinsky, S. Mordechai, and M. Huleihel, "FTIR microspectroscopy of malignant fibroblasts transformed by mouse sarcoma virus," *J. Biochem. Biophys. Methods* **55**(2), 141–153 (2003).
37. V. Erukhimovitch, M. Talyshinsky, Y. Souprun, and M. Huleihel, "Spectroscopic characterization of human and mouse primary cells, cell lines and malignant cells," *Photochem. Photobiol.* **76**, 446–451 (2002).
38. J. Ball, J. McCarter, and S. Sunderland, "Evidence for helper independent murine sarcoma virus. I. Segregation of replication defective and transformation defective viruses," *Virology* **56**, 268–284 (1973).
39. S. Wartewig, *IR and Raman Spectroscopy*, pp. 75–122, John Wiley and Sons, New York (2003).
40. B. Everitt, *Cluster Analysis*, John Wiley and Sons, New York (1980).
41. C. Huberty, *Applied Discriminant Analysis*, John Wiley and Sons, New York (1994).
42. R. A. Fisher, "The use of multiple measures in taxonomic problems," *Ann. Eugenics* **7**, 179–188 (1936).
43. F. S. Parker, *Application of Infrared Spectroscopy in Biochemistry,*

Biology and Medicine, Plenum, New York (1971).
44. D. Naumann, "FT-infrared and FT-Raman spectroscopy in biomedical research," *Appl. Spectrosc. Rev.* **36**, 239–298 (2001).
45. E. Benedetti, E. Bramanti, F. Papineschi, I. Rossi, and E. Benedetti, "Determination of the relative amount of nucleic acids and proteins in leukemic and normal lymphocytes by means of Fourier transform infrared microspectroscopy," *Appl. Spectrosc.* **51**, 792–797 (1997).
46. J. Mourant, K. W. Short, S. Carpenter, N. Kunapareddy, L. Coburn, T. M. Powers, and J. P. Freyer, "Biochemical differences in tumorigenic and nontumorigenic cells measured by Raman and infrared spectroscopy," *J. Biomed. Opt.* **10**(3), 031106 (2005).
47. K. W. Short, S. Carpenter, J. P. Freyer, and J. Mourant, "Raman spectroscopy detects biochemical changes due to proliferation in mammalian cell cultures," *Biophys. J.* **88**, 4274–4288 (2005).
48. L. M. McIntosh, M. Jackson, H. H. Mantsch, M. F. Stranc, D. Pilavdzic, and A. N. Crowson, "Infrared spectra of basal cell carcinomas are distinct from non-tumor-bearing skin components," *J. Invest. Dermatol.* **112**, 951–956 (1999).
49. T. Gao and Y. Ci, "Fourier transform infrared spectroscopic features of human breast benign and malignant tissues," *Internet J. Vibrational Spectrosc.* **3**(5) (1999).
50. R. K. Sahu, S. Argov, A. Salman, U. Zelig, M. Huleihel, N. Grossman, J. Gopas, J. Kapelushnik, and S. Mordechai, "Can vibrational spectroscopy at higher wavenumbers (midIR) shed light on universal biomarkers for carcinogenesis in tissues?" *J. Biomed. Opt.* **10**(5), 054017 (2005).
51. B. Rigas, S. Morgello, I. S. Goldman, and P. T. Wong, "Human colorectal cancers display abnormal Fourier-transform infrared spectra," *Proc. Natl. Acad. Sci. U.S.A.* **87**, 8140–8144 (1990).
52. P. G. Andreus, "Cancer monitoring by FTIR spectroscopy," *Technol. Cancer Res. Treat.* **5**(2), 157–167 (2006).
53. C. Dombi, J. Banoczy, M. Kramer, W. P. Wertz, and A. C. Squier, "Study of the permeability of oral leukoplakia," *Fogorv. Sz.* **92**(5), 137–142 (1999).
54. F. Lang, M. Ritter, E. Woll, H. Weiss, D. Haussinger, J. Hoflacher, K. Maly, and H. Grunicke, "Altered cell volume regulation in ras oncogene expressing NIH fibroblasts," *Pfluegers Arch.* **420**(5–6), 424–427 (1992).
55. D. C. Malins, ■ Johnson, E. A. Barker, N. L. Polissar, T. M. Wheeler, and K. M. Anderson, "Cancer-related changes in prostate DNA as men age and early identification of metastasis in primary prostate tumors," *Proc. Natl. Acad. Sci. U.S.A.* **100**(9), 5401–5406 (2003). AQ: #3
56. V. R. Kondepati, M. Keese, H. M. Heise, and J. Backhaus, "Detection of structural disorders in pancreatic tumour DNA with Fourier-transform infrared spectroscopy," *Vib. Spectrosc.* **40**, 33–39 (2006).
57. R. K. Sahu, S. Argov, A. Salman, M. Huleihel, N. Grossman, Z. Hammody, J. Kapelushnik, and S. Mordechai, "Characteristic absorbance of nucleic acids in the mid-IR region as possible common biomarkers for diagnosis of malignancy," *Technol. Cancer Res. Treat.* **3**(6), 629–638 (2004).
58. Z. Hammody, R. K. Sahu, S. Mordechai, E. Cagnano, and S. Argov, "Characterization of malignant melanoma using vibrational spectroscopy," *Scientific World J.* **5**, 173–182 (2005).
59. P. G. Andreus and R. D. Strickland, "Cancer grading by Fourier transform infrared spectroscopy," *Biospectroscopy* **4**(1), 37–46 (1998).
60. C. Liu, Y. Zhang, X. Yan, X. Zhang, C. Li, W. Yang, and D. Shi, "Infrared absorption of human breast tissues in vitro," *J. Lumin.* **119–120**, 132–136 (2006).
61. Y. Tong and Y. Lin, "FTIR study on the normal and cancerous stomach tissues," *Guangpuxue Yu Guangpu Fenxi* **21**(3), 324–327 (2001).
62. N. Fujioka, Y. Morimoto, T. Arai, K. Takeuchi, M. Yoshioka, and M. Kikuchi, "Differences between infrared spectra of normal and neoplastic human gastric cells," *Spectroscopy (Amsterdam)* **18**, 59–66 (2004). AQ: #4
63. D. Mihailovic, B. Dordevic, and V. Mihailovic, "Nuclear volume in type I gastric intestinal metaplasia," *Anal Quant Cytol. Histol.* **21**(2), 143–144 (1999).
64. R. Drezek, M. Guillaud, T. Collier, I. Boiko, A. Malpica, C. Macaulay, M. Follen, and R. Richards-Kortum, "Light scattering from cervical cells throughout neoplastic progression: influence of nuclear morphology, DNA content, and chromatin texture," *J. Biomed. Opt.* **8**(1), 7–16 (2003).

AUTHOR QUERIES — 021702JBO

#1 Ref. 9: “Paris” ok?
#2 Ref. 14: “Paris” ok?
#3 Ref. 55: Please provide first initial of author Johnson.
#4 Ref. 62: Spectroscopy (Amsterdam), Spectroscopy (Eugene, Or.), or Spectroscopy Europe?